Isotopomer Fractionation in the UV Photolysis of N₂O: 3. 3D Ab Initio Surfaces and Anharmonic Effects[†]

Wei-Chen Chen,† Shinkoh Nanbu,‡ and R. A. Marcus*,†

Noyes Laboratory, 127-72, California Institute of Technology, Pasadena, California 91125, and Department of Materials & Life Sciences, Faculty of Science & Technology, Sophia University, 7-1 Kioi-cho, Chiyoda-ku, Tokyo 102-8554, Japan

Received: February 24, 2010; Revised Manuscript Received: May 13, 2010

The wavelength-dependent isotopic fractionation of N_2O is calculated, extending our previous work, Parts 1 and 2, in several aspects: (1) the fully three-dimensional ab initio electronic potential and transition dipole moment surfaces of S. Nanbu and M. S. Johnson (*J. Chem. Phys. A* **2004**, *108*, 8905) are used to calculate the absorption cross sections, instead of a 2D surface and (2) the vibrational frequencies and wave functions with anharmonicity correction are used for the ground electronic state. The results for the absorption spectrum and for the isotopic fractionation of the different isotopomers are discussed. One difference between experiments measuring the absorption coefficient (von Hessberg et al. *Atmos. Chem. Phys.* **2004**, *4*, 1237) and the others that measure instead the photodissociation is also discussed. Experiments on the quantum yield for wavelengths longer than 200 nm (>50 000 cm $^{-1}$) would be helpful in treating the observed difference.

Theory.

Introduction

 N_2O is the dominant anthropogenic ozone-depleting substance being emitted in the 21st century.¹ It is also a key greenhouse gas and has a long lifetime in the troposphere.² When it reaches the stratosphere, where it is no longer shielded by ozone, it dissociates photochemically and attacks the ozone layer.^{1,2} Isotopic studies provide a way of distinguishing anthropogenic sources of N_2O from the natural sources.^{2,3}

Isotopic fractionation in the photolysis of N₂O in Earth's atmosphere is dominated mainly by the low energy side of the peak of the absorption cross section (ca. 47 500–50 000 cm⁻¹). This photolysis process has been extensively studied,⁴ and various authors, including von Hessberg et al.5 and McLinden et al.,6 have discussed atmospheric implications, which are also summarized in Parts 17 and 2.8 In our earlier theoretical studies, 7,8 the results of the vibrational analysis were used to calculate the vibrational frequencies and wave functions in the ground state. Using the multidimensional reflection principle, ^{4,9} the absorption spectrum and the isotopic fractionation were calculated as a function of wavelength. In Part 1,7 there were comparisons with other theories, in particular, the timedependent (wave packet) studies by Johnson et al., 10 and Nanbu and Johnson¹¹ and the prediction from the zero-point vibrational energy by Yung and Miller.12

The calculated absorption cross section by Chen et al.⁸ gave reasonable agreement with experiments in the important region, the low energy side of the peak;⁸ however, there was still some discrepancy with experiment in this lower energy region (<48 000 cm⁻¹). In the present paper, the method of Part 2 is extended in two respects: (1) using the 3-dimensional ab initio electronic potential and transition dipole moment surfaces calculated by Nanbu and Johnson¹¹ and (2) including the anharmonicity of the ground electronic state that is obtained

from the experimental rovibrational spectra.¹³ The present treatment improves the calculated absorption cross section in

the low-energy region and improves somewhat the wavenumber

Absorption Cross Section. The theoretical procedure used

to obtain absorption cross sections for the N2O isotopomers is

similar to that we described previously, but with the additions

described below. UV photolysis of N₂O in the spectral region

of interest is essentially a direct dissociation, since the absorption

spectrum is a broad envelope with only a weak structure

superimposed. As before, the time-dependent expression for the

absorption cross section can be rewritten in a time-independent

form using the Franck-Condon principle^{4,9} (known as the

reflection principle when the upper electronic state is repulsive).

The absorption cross section, σ , to an upper electronic state, f,

dependence of the photolysis fractionation.

where **R** and **Q** denote internal and normal coordinates, respectively. The relation between these coordinates is that **R** = \mathcal{L} **Q**, where \mathcal{L} is a matrix composed of eigenvectors of the \mathscr{GF} matrix. Here \mathscr{G} and \mathscr{F} matrices of N₂O are given in the Appendix. It is useful to note that the normal coordinates **Q** and the vibrational wave function, Ψ_n , in eq 1 are slightly different among isotopomers and that both differences contribute to the vibrational effect¹⁵ in the absorption cross section of isotopomers.

In eq 1, the difference in slopes $\Delta S(\omega)$ of the potential energy difference at ω is given by

is given by $\sigma_{fn}(\omega) = \frac{\pi\omega}{\hbar\varepsilon_0c} \frac{1}{2\pi} \int_{-\infty}^{\infty} \mathrm{d}t \, \langle \Psi_n | \pmb{\mu}_{fi}^{\dagger} \mathrm{e}^{-iH_itl\hbar} \pmb{\mu}_{fi} | \Psi_n \rangle \mathrm{e}^{i(\omega + E_i/\hbar)t}$

 $[\]approx \frac{\pi\omega}{3\varepsilon_0 c} \int d\mathbf{Q} |\Psi_n(\mathbf{Q})|^2 |\boldsymbol{\mu}_{fi}(\mathbf{R})|^2 \delta(\hbar\omega - V_f(\mathbf{R}) + V_i(\mathbf{R}))$ $\approx \frac{\pi\omega}{3\varepsilon_0 c} \int dq_1 \dots dq_{N-1} |\Psi_n(\mathbf{Q})|^2 |\boldsymbol{\mu}_{fi}(\mathbf{Q})|^2 /\Delta S(\omega)$ (1)

where \mathbf{R} and \mathbf{Q} denote internal and normal coordinates, respectively ⁸ The relation between these coordinates is that \mathbf{R}

[†] Part of the "Reinhard Schinke Festschrift".

^{*} To whom correspondence should be addressed E-mail: ram@caltech.edu.

[†] California Institute of Technology.

[‡] Sophia University.

$$\Delta S(\omega) = (\partial [V_i(\mathbf{Q}) - V_f(\mathbf{Q})]/\partial q_N)_{q_N}$$
 (2)

In eq 1, $\mu_f(\mathbf{R})$ is the vector of the transition dipole moment function for a transition between the ground and the excited electronic states, i and f, respectively; $V_i(\mathbf{Q})$ and $V_f(\mathbf{Q})$ denote their potential energy surfaces; and q_N is any coordinate for which $V_f(\mathbf{Q}) - V_i(\mathbf{Q})$ is a monotonic function of q_N and avoids any singularity in eq 1. We have chosen q_N to be the massweighted cosine of the bending angle. As seen in Figure 1, this variable fulfills the essential criterion for the choice of q_N , namely that the $V_f - V_i$ be a monotonic function of q_N . The result of integrating q_N is independent of the choice of coordinate. The specific q_N value in eq 2 is obtained by solving the equation for q_N that the absorbed photon energy $\hbar \omega$ equals the vertical potential energy difference of the two electronic states:

$$\hbar\omega = V_{f}(q_{1}, \dots, q_{N-1}, q_{N}) - V_{i}(q_{1}, \dots, q_{N-1}, q_{N})$$
for any (q_{1}, \dots, q_{N-1}) (3)

In eq 1, both the coordinate and momentum aspects of the classical Franck—Condon principle are used. It was also used in Part 2,8 but differs from that used in Part 1, which set $\hbar\omega = V_f - E_g^0/2$,7 where E_g^0 is the zero-point energy of the ground electronic state. Both alternatives are approximate. Equation 1 has the merit of being the unperturbed term in a systematic semiclassical perturbation expansion of the electronic transition probability extending the application of the classical Franck—Condon principle. The Equation 1 also happens to give a better agreement with the red side of the experimental absorption cross section than an alternative form of the Franck—Condon principle used in Part 1.7

The n in eq 1 refers to the totality of quantum numbers of the several vibrational coordinates. The best currently available 3-dimensional ab initio potential energy surfaces ($V_i(\mathbf{R})$) and $V_f(\mathbf{R})$), and the transition dipole moment ($\mu_{fi}(\mathbf{R})$) surface appear to be those of Nanbu and Johnson. (The grids and the values of these potential energy and transition moment surfaces used in the present calculation were corrected for some accidental errors and are given in the Supporting Information.) These surfaces are given in terms of mass-dependent Jacobi coordinates, which are varied in all degrees of freedom, instead of the surfaces with fixed NN distance used in our previous treatments. (8.18)

In the present calculation of the absorption cross section, the effect of vibrational anharmonicity in the ground electronic state i is included using a variational method for the vibrational wave functions, $\Psi_n(\mathbf{Q})$, instead of the harmonic vibrational wave functions used previously.⁸ Although anharmonicity has little effect on the total absorption cross section near the peak region, it does affect the absorption cross section in the low energy region and so has some effect on the wavelength-dependence of the isotopic fractionation there.

The total absorption cross section, $\sigma_{\text{total}}(\omega, T)$, for any absorption frequency, ω , is temperature-dependent due to the thermal effect on the population on the initial vibrational states. It is given in terms of the individual $\sigma_{fn}(\omega)$ for the initial vibrational states n at temperature T to an upper electronic state f,

$$\sigma_{\text{total}}(\omega, T) = \sum_{n} \sigma_{fn}(\omega) \exp\left(\frac{-(E_n - E_0)}{k_{\text{B}}T}\right) / Q_{\text{vib}}(T)$$
(4)

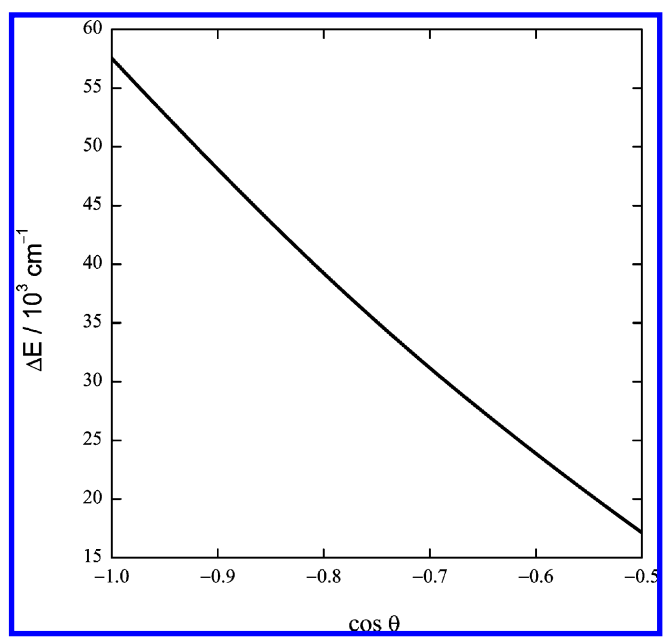


Figure 1. The energy difference, ΔE between the ground and excited electronic states as a monotonic function of $\cos(\angle NNO)$. A mass-weighted $\cos(\angle NNO)$ is the q_N used in eq 2. For the present plot only, the bond length of the NN and NO bonds was fixed in the equilibrium distances of the N₂O molecule in the ground electronic state.

where $Q_{vib}(T)$ is the partition function of the vibrations in the ground electronic state, and E_n and E_0 are the vibrational energy of the vibrational state n and zero-point energy, respectively. An anharmonic effect on E_n is also included using the variational method. Therefore, in addition to eq 1, the exponential weighting divided by the partition function in eq 4 also contributes a vibrational effect in the total absorption cross section among isotopomers. The vibrational states, n, with energy less than 1500 cm⁻¹ above the zero-point energy are included. They involve the ground state, the first vibrationally excited state of NO stretching, and the first and second excited states of the N₂O bending. Since N₂O is linear in the electronic ground state, its bending vibration is doubly degenerate, as discussed in Part 1.7 In the present calculation for the total absorption cross section of N₂O, only excitation from the ground electronic state to the first excited state, $2A'(1\Delta)$ is considered, since the second excited state, $1A''(1\Sigma^{-})$, has little effect on the absorption cross section and fractionation, as discussed in Part 2.8

Variational Method. In the variational method used to obtain the vibrational wave functions, $\Psi_n(\mathbf{Q})$, in eq 1 with the anharmonicity correction, the trial functions are a linear combination of the harmonic wave functions

$$\Psi_n(\mathbf{Q}) = \sum_m c_{n,m} \, \Phi_m^{(0)}(\mathbf{Q}) \tag{5}$$

where $\Phi_m^{(0)}(\mathbf{Q})$ are the normalized harmonic wave functions of three modes and are given in the Appendix. The $c_{n,m}$ coefficients are obtained from the eigenvectors of the secular determinant. Since an orthonormal basis set is used, the secular determinant is

$$\begin{vmatrix} H_{1,1} - E & H_{1,2} & \cdots & H_{1,n} \\ H_{2,1} & H_{2,2} - E & \cdots & H_{2,n} \\ \vdots & \vdots & \ddots & \vdots \\ H_{n,1} & H_{n,2} & \cdots & H_{n,n} - E \end{vmatrix} = 0$$
 (6)

TABLE 1: The Calculated and Experimental Energy Difference between the Ground and First-Excited Vibrational States in Each Normal Mode of Various Isotopomers^a

isotopomer	$\overline{ u}_1$	$\overline{ u}_1^{ ext{exptl }32}$	$ar{ u}_2$	$\overline{\nu}_2^{\text{exptl } 33,34}$	$\overline{ u}_3$	$\overline{\nu}_3^{ ext{exptl }35}$
446	2222.327	2223.757	1284.932	1284.903	588.356	588.768
447	2218.686	2220.074	1264.698	1264.704	585.962	586.362
448	2215.366	2216.711	1246.833	1246.885	583.836	584.225
456	2176.213	2177.657	1280.409	1280.354	575.027	575.434
546	2200.233	2201.605	1269.923	1269.892	584.915	585.312
556	2153.335	2154.726	1265.381	1265.334	571.501	571.894

^a Due to anharmonicity, the harmonic normal mode frequencies may be slightly larger than the values provided here. The unit is in cm⁻¹.

where $H_{i,j} = \langle \Phi_i^{(0)} | H | \Phi_j^{(0)} \rangle$. The Hamiltonian H includes the harmonic vibrational operator and potential terms higher than the quadratic, which are obtained by Teffo and Chédin¹³ by fitting to rovibrational experimental data. The *j*th eigenvalue for eq 6 corresponds to the vibrational energy E_i of the Ψ_j state.

The largest first anharmonic terms of two stretching modes are larger than those involving the bending mode by a factor of ~ 4 , 13 and the frequency of the bending mode is much smaller than that of the two stretching modes. Therefore, in the variational treatment, the bending mode energies converge faster than the two stretching ones. To have similar accuracy for all modes and to complete the calculations in a reasonable computational time, the basis set in the variational method included six harmonic wave functions for each stretching vibration, and four nondegenerate ones for the bending vibration (i.e., $6 \times 6 \times 4 = 144$ harmonic wave functions in the orthonormal basis set).

Calculated Isotopic Fractionation. The expression for the photodissociation rate at energy $\hbar\omega$ shows a dependence on three factors: the total absorption cross section $\sigma_{\text{total}}(\omega)$ in eq 4, the photon flux, and the quantum yield of the photodissociation. The isotopic fractionation $\varepsilon(\omega)$ of one isotopomer relative to another due to a direct photodissociation reaction can be defined in terms of the ratio of photodissociation rates,

$$\varepsilon(\omega) = \left[\frac{\sigma'_{\text{total}}(\omega)}{\sigma_{\text{total}}(\omega)} - 1 \right] \times 1000\%$$
 (7)

where $\sigma'_{\text{total}}(\omega)$ is the total absorption cross section of an isotopomer.

When the upper state is repulsive without any readily accessible curve crossing, the quantum yield equals unity for all the isotopomers, and then the isotopic fractionation $\varepsilon(\omega)$ for the reaction products can also be expressed in terms of this ratio of total absorption cross sections.

One can also define a quantity,

$$^{17}\Delta_{\varepsilon} = \varepsilon^{447} - 0.515 \times \varepsilon^{448} \tag{8}$$

where a deviation from zero is a measure of an "anomalous" isotope effect. It is often also called a "mass-independent" isotope effect, although the latter term is less ambiguously used when it refers to the case of a slope of unity for a three-isotope plot of the oxygen isotopes. In N_2O , the experimental mass-dependent slope is 0.515.3

Results

Absorption Cross Section. The energy difference between the ground and first-excited vibrational states of each of the modes obtained by the variational method is given in Table 1.

Using these vibrational energies, the calculated absorption cross section with the variational energy of the most abundant isotopomer, 446, is shown in Figure 2. The improvement in absorption cross section due to the variational method and the 3-dimensional ab initio surfaces is best seen in Figure 2b for the red side of the absorption band. The blue side is of less interest in atmospheric isotopic fractionation^{5,19–23} and may have additional contributions from higher electronic states.

Isotopic Fractionation. Using eq 7 with the absorption cross section of various isotopomers, the wavelength-dependent fractionation of isotopomers 546, 556, and 456 were calculated relative to the most abundant isotopomer 446 for 283 and 233 K, the temperatures for which experimental data are available. The results are shown in Figures 3, 4, and 5. The isotopic fractionation at these two temperatures is helpful in the three-dimensional chemistry-transport model in studying the stratospheric enrichment of the isotopically heavy N₂O. The calculated fractionation for 447 and 448 relative to 446 at 283 K is given in Figure 6.

Discussion

Cross Sections. Using the experimental force constants listed in the Appendix with no adjustable parameters, the vibrational energy differences ("vibrational frequencies") obtained by the variational method for the anharmonicity is in reasonable agreement with experiment: The difference of the two with no adjustable parameter is <1.5 cm⁻¹ in all modes, as seen in Table 1. The values are used in eq 4 in obtaining the total absorption cross section at various temperatures.

To facilitate this comparison with the experimental spectrum for the long wavelength region (180–220 nm) where the isotopic fractionation is of most interest, the calculated peak was rescaled in amplitude by a factor of 1.59 to match the maximum absorption (\sim 1.4 \times 10⁻¹⁹ cm²) in experiments^{5,24} and was redshifted by 800 cm⁻¹ to match the maximum absorption at \sim 5.5 \times 10⁴ cm⁻¹ and the majority of the rising part (\sim 5.0–5.5 \times 10⁴ cm⁻¹) in experiments.^{5,24} No further adjustments were then used to calculate the isotopic fractionation of the different isotopomers.

As mentioned in Part 2,⁸ the need for the shift arises from a small error in the absolute energy difference between the energy of ground and excited electronic states, an error common in ab initio calculations. Only the absorption data of 14 N₂O, not the isotopic fractionation, is used in this shift. A rescaling in height is also not unexpected, since the ab initio calculation of the absolute transition dipole moment μ_{fi} has some error.^{25,26} However, we note that the rescaling of the amplitude factor at the absorption maximum has no effect on the isotopic fractionation, since the factor cancels in eq 7. The fact that this amplitude scaling is close to unity is a tribute to the electronic structure calculations of Nanbu and Johnson.¹¹ The total

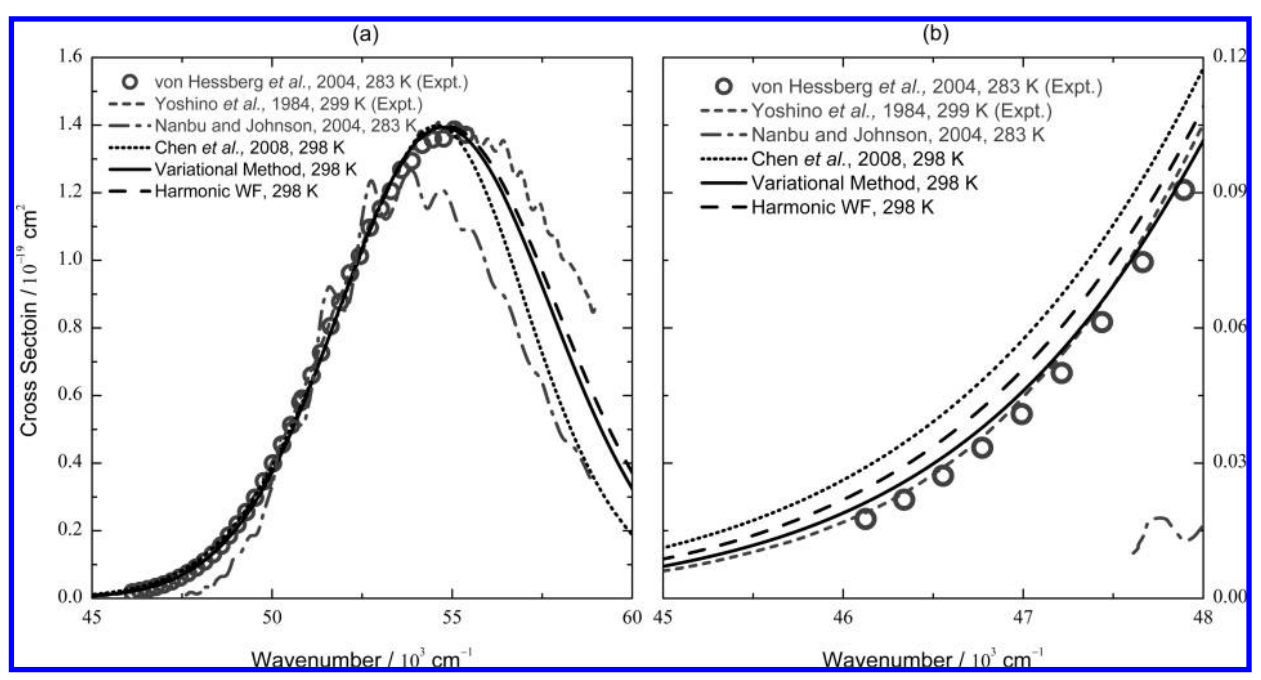


Figure 2. Absorption cross section of ¹⁴N¹⁴N¹⁶O. (a) The calculated results are rescaled and shifted to overlap with experimental data at the longer wavelength region. (b) An enlargement of panel a in the lower wavelength region.

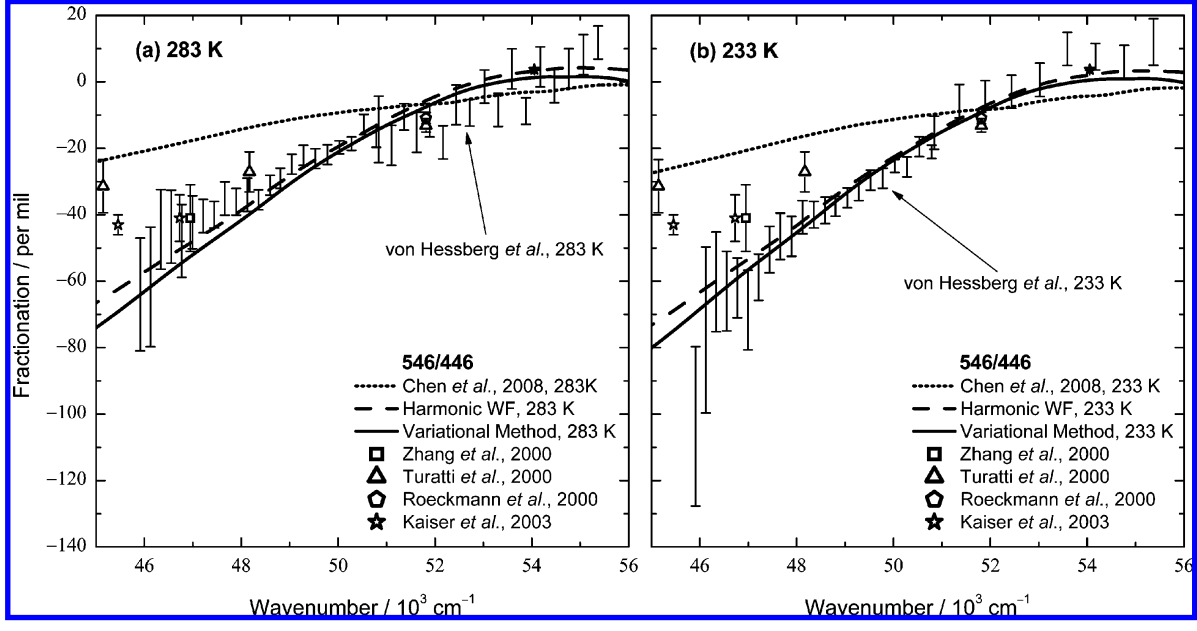


Figure 3. Fractionation of 546 calculated at 233 and 283 K and experimental points.

absorption cross sections for other isotopomers are calculated similarly using the same shift in the peak position as that for 446, since the energy difference between potential energy surfaces is independent of isotopic substitution. This red shifting of the absorption maximum also has a minor effect on the calculated isotopic fractionation.

Although the current calculation of the absorption cross section shows a good agreement with experiments on the red side, it is somewhat too low on the blue side, as seen in Figure 2. The discrepancy may be due to the assumption of the Franck-Condon principle, and a calculation with higher-order terms for the approximate calculation of the absorption cross section than that in eq 1 will be helpful in resolving this issue. In the meanwhile we note that the isotopic fractionation of atmospheric interest in the photolysis of N2O is dominated by the red side of the absorption peak.

Comparison of Calculated Absorption Cross Sections. In the variational calculation of vibrational wave functions in the ground electronic state, the convergence of the basis set in the variational method was also tested by using a larger basis set to calculate the vibrational wave functions in the most abundant isotopomer, 446. The new basis set included eight harmonic wave functions for each stretching vibration and six nondegenerate ones for the bending vibration. There are thus $8 \times 8 \times 6$, or 384, orthonormal wave functions in the basis set. There is negligible difference (<0.3%) in the absorption cross section between the larger and smaller basis sets (both rescaled by 1.59 and red-shifted by 800 cm⁻¹). Accordingly, the smaller basis set is also expected to be adequate for the isotopic fractionation, and was used in the remaining calculations.

The absorption cross section obtained using the ab initio 3-dimensional surfaces with *harmonic* wave functions is also

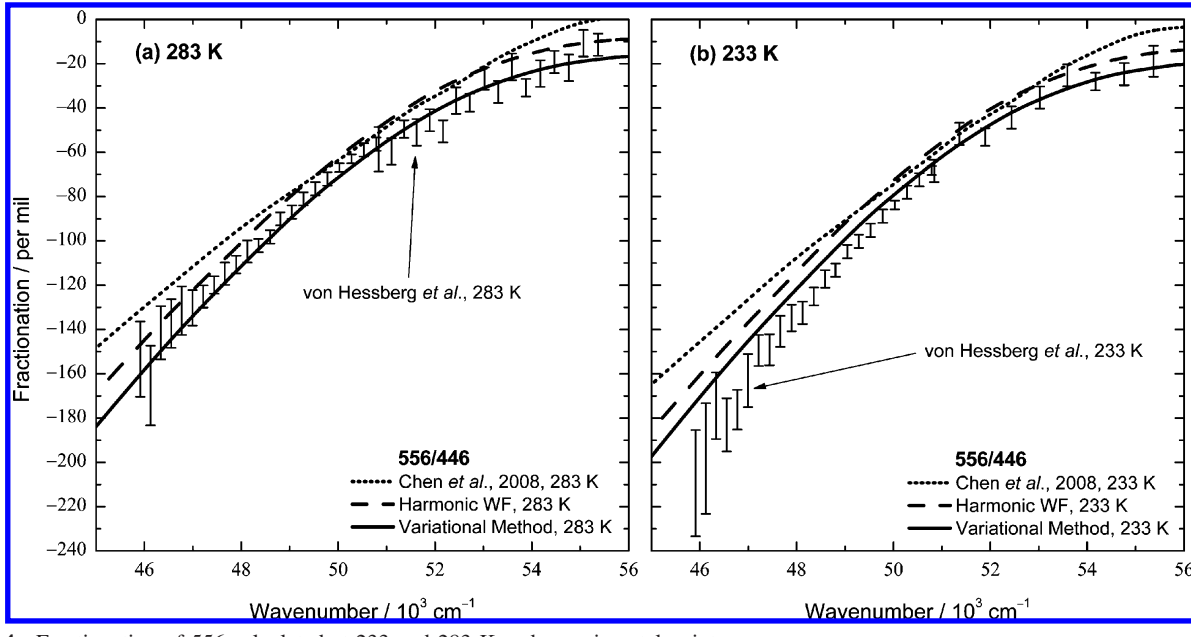


Figure 4. Fractionation of 556 calculated at 233 and 283 K and experimental points.

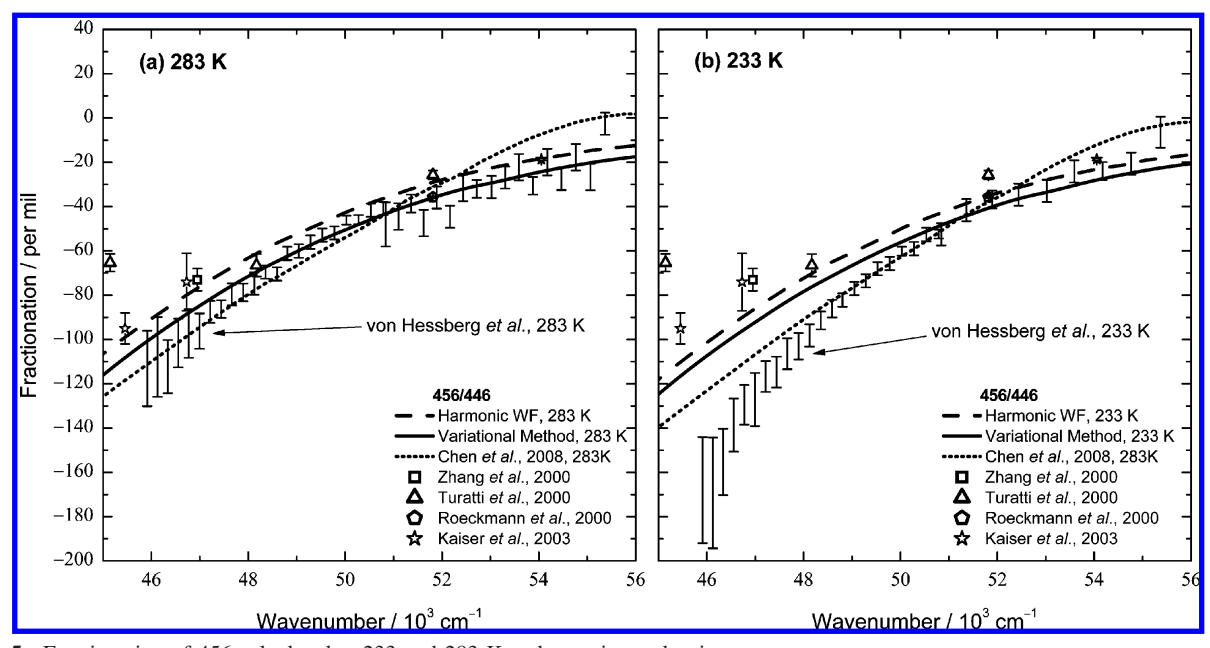


Figure 5. Fractionation of 456 calculated at 233 and 283 K and experimental points.

shown in Figure 2, in addition to the present result with the anharmonic potentials. Its rescaled and red-shifted parameters are 1.56 and 900 cm⁻¹, respectively. The slightly difference in the rescaled and red-shifted parameters between harmonic and anharmonic ones is due to the slight changes in the wave functions in the variational treatment. In addition to errors in ab initio surfaces, vibrational wave functions also have a minor effect on the red-shifted parameter. Compared with the absorption cross section obtained by the anharmonic variational wave functions, the harmonic ones give comparable results near the peak region, as expected, but in the low-energy region, the absorption cross section with the harmonic treatment is larger than that with the anharmonic one and not in as good agreement with the experimental results, 5.24 as seen in Figure 2b.

In Part 2,8 the absorption cross section was obtained using harmonic wave functions and more approximate 3-dimensional potential surfaces: It was assumed that the NN distance contributes only the harmonic terms on the potential energy

surfaces and has no effect on the transition dipole moment function. We note that even with 3-dimensional ab initio surfaces, the current eq 1 does not attempt to give an absorption cross section with state-resolved products. It does not treat the dynamics beyond the initial stage of the dissociation. For example, because the initial electronic state of N_2O is linear and the excited state is bent, N_2 is produced in a highly excited rotational state, whereas the N_2 vibration is largely produced in its ground vibrational state. 27

Nanbu and Johnson used a wave packet propagation on the three-dimensional potential energy surface to calculate the UV absorption cross sections of $N_2O.^{11}$ It is a quantum treatment and, in principle, a more accurate method than that used here. However, compared with the experimental data, the calculated absorption cross section was too narrow, as shown in Figure 2, perhaps due to cumulative numerical errors. In any case, the large deviation in the absorption cross section in the lower energy region precludes the wave packet-calculated isotopic

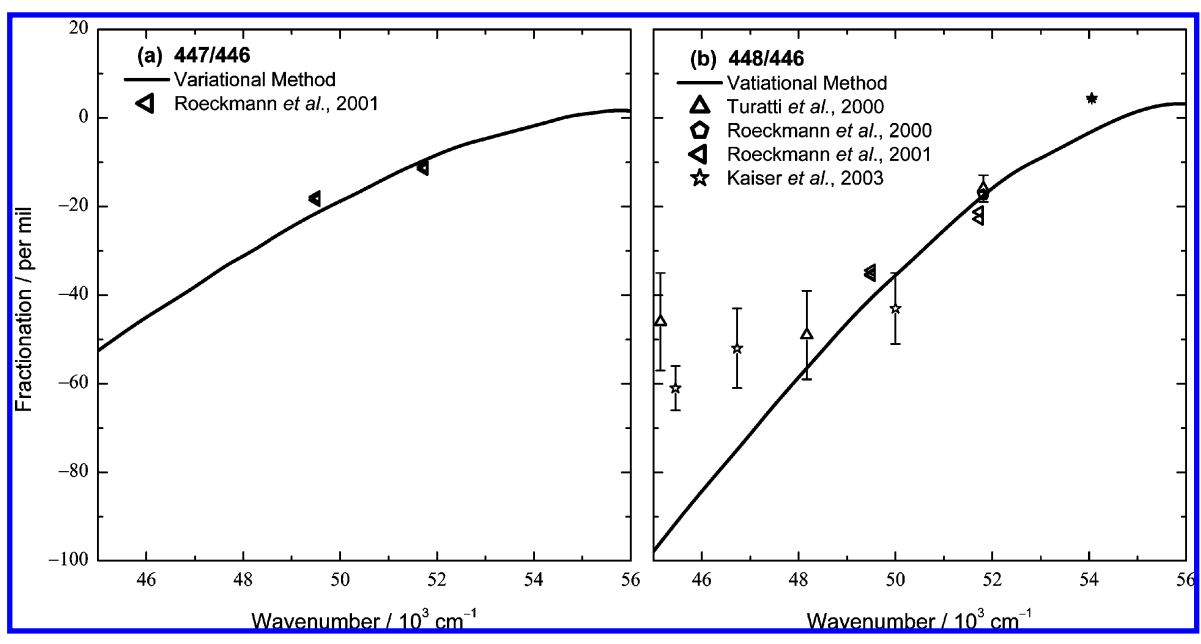


Figure 6. Fractionation of 447 (a) and 448 (b) calculated at 283 K and experimental points.

fractionation from agreeing well with experiment. 11 Improved wave packet calculations will clarify the accuracy of the presently used Franck-Condon principle.

Experimental Isotopic Fractionation. Two methods of measuring an experimental wavelength-dependent isotopic fractionation have been employed in the literature. One method is the direct measurement of the residual N2O after photolysis at various wavelengths, as in Zhang et al., 19 Turatti et al., 20 Röckmann et al.,^{21,22} and Kaiser et al.²³ In the other method, the relative absorption cross section for the isotopomers at various wavelengths is measured, as in von Hessberg et al.⁵ Agreement between the two methods involves the assumption that the quantum yield is unity. Near the maximum of the absorption cross section the experimental quantum yield is, indeed, almost unity.²⁸ However, in the longer wavelength region, where isotopic fractionation is of particular interest, the quantum yield may be slightly different between isotopomers if other processes compete because of the smaller internal energy available for direct dissociation and perhaps reflecting a role for any crossing of the potential energy surfaces. The competing processes may result from (1) collision between a potentially long-lived excited N₂O and the bath gases, (2) fluorescence from such an excited state to ground state, and (3) interstate crossing (avoided crossing) of the electronic excited states. Any of these possibilities may explain why the isotopic fractionation in the absorption spectra of 456 and 546 obtained in the experiments of von Hessberg et al.5 is lower than the experimental fractionation measured by the reaction yields 19-21,23 at the longer wavelengths, as seen in Figure 3 and 5.

Comparison of Experimental and Calculated Isotopic **Fractionation.** The wavelength-dependent fractionation of isotopomers 546, 556, and 456 calculated relative to the most abundant isotopomer 446 is shown in Figures 3-5. Our calculated results are most directly comparable with the result obtained by von Hessberg et al.⁵ in the longer wavelength region, since both fractionations are estimated from the ratio of the absorption cross sections and are, therefore, independent of any assumption about the quantum yield.

Compared with the calculated fractionation in Part 2,8 the current fractionation at energies lower than 50 000 cm⁻¹ shows a significant improvement for 546 (Figure 3) and marginal improvement for 556 (Figure 4), but slightly worse for 456 (Figure 5). The calculated fractionation for 447 and 448 relative to 446 at 283 K is given in Figure 6. At wavenumbers larger than 50 000 cm⁻¹, both calculated results agree with experiment. No absorption spectral data appear to be available for 447 and 448 in the longer wavelength region. It would be interesting to measure that wavelength-dependent fractionation of oxygen isotopomers using the method of von Hessberg et al.⁵ as well as to determine experimentally the quantum yields of photodissociation at wavelengths longer than 200 nm (50 000 cm⁻¹), as noted earlier.

The current results, in which the more approximate treatment of the NN-stretching coordinate in Part 28 is avoided, are more accurate and in better overall agreement with experiment. Compared with the harmonic treatment, the variational treatment with the anharmonic potential gave marginal improvement at the lower temperature, 233 K. The experimental fractionation of all isotopomers has a larger temperature dependence than the calculations, as seen in Figures 3-5. One possibility is the different couplings between the excited electronic and rotational states, which is not included in the current treatment. Further theoretical and experimental studies may be helpful in understanding this behavior. The sensitivity of the calculated fractionation to changes in the wavelength is $556 > 456 > 448 \ge$ $546 \gtrsim 447$, which is similar to the results from experiments.^{5,19–23}

Three-Isotopic Fractionation Plot. The three-isotope plot of the fractionations ε^{447} vs ε^{448} is shown in Figure 7a, where the calculated results give a good agreement with the sparse experimental data obtained by Röckmann et al.²² The slope of our results on the three-isotope plot is 0.537, which is slightly larger than the mass-dependent coefficient (0.515) obtained by analyzing a range of commercial N₂O gases.³ In Figure 8, a plot of the multi-isotope correlations of the fractionation 448 vs the average fractionations of 546 and 456 is shown. The calculated and experimental results agree; however, the experiments give a slightly larger slope in the correlations in the large fractionation region.

The departure from the mass-dependent fractionation of the O in N₂O is given by $^{17}\Delta$,

$$^{17}\Delta = \delta^{447} - 0.515 \times \delta^{448} \tag{9}$$

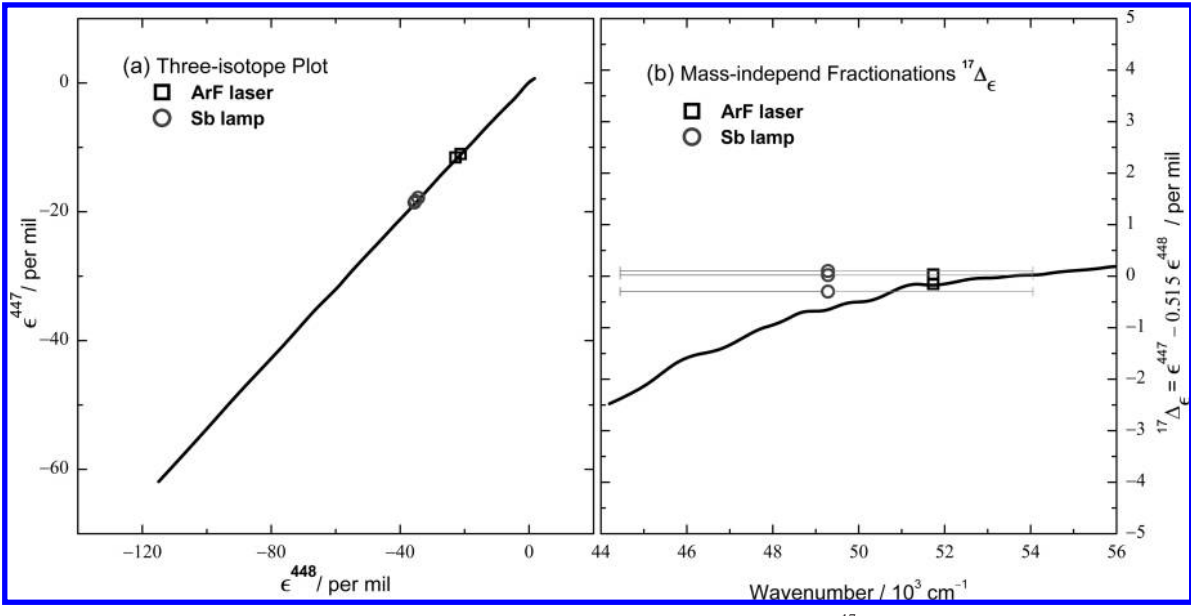


Figure 7. (a) The three-isotope plot of fractionations 447 vs 448. (b) The wavenumber-dependent $^{17}\Delta_{\epsilon}$. The experimental data on both plots were obtained by Röckmann et al. 22 The error bars on panel b indicate the energy range of the Sb lamp emit. The open circles are at the peak intensity of the emission.

where the δ 's are the enrichments of the specified isotopomer, defined as

$$\delta = \left[\frac{\left(\frac{[O']}{[O]} \right)_f}{\left(\frac{[O']}{[O]} \right)_i} - 1 \right] \times 1000\%$$
 (10)

where the prime indicates the isotope. The i and f subscripts indicate the measured ratios of the initial and the remaining N₂O, respectively. Since the N₂O photolysis is a single-step reaction with a nearly unit quantum yield, it is straightforward to obtain the approximate relation between the fractionation ϵ and the enrichment δ as²⁹

$$\delta \approx \delta_0 + \varepsilon \times \ln f \tag{11}$$

where f is the fraction of N_2O remaining after photolysis. δ and δ_0 are the residual and initial enrichments, respectively. Using the definition in eq 10, the δ_0 value is zero. Therefore, the key quantity $^{17}\Delta$ in eq 9 is approximately proportional to $^{17}\Delta_\varepsilon$ in eq 8, differing by a factor of $\ln f$.

The calculated wavenumber dependence of the massindependent $^{17}\Delta_{\epsilon}$, given in Figure 7b, shows a nearly "normal" isotopic mass dependence ($^{17}\Delta_{\epsilon}\approx 0$) in the higher-energy region ($\gtrsim\!51~000~\text{cm}^{-1}$) and a minor anomaly in the lower-energy region. Our calculations in Figure 7b agree with measurements obtained by using the ArF laser at 193 nm (52 000 cm $^{-1}$). 22 A Sb lamp covers both the normal and the anomalous regions. Because a larger absorption cross section of the N_2O photolysis in the normal region, the "anomalous" fractionation may not be observed in the photolysis with a Sb lamp. 22 The convolution of the N_2O absorption cross section with the atmosphere UV transmission window shows that the peak of atmospheric N_2O photolysis occurs around 200 nm (50 000 cm $^{-1}$); 30 however, the width of the UV transmission window in the atmosphere could obscure any anomalous isotopic fractionation.

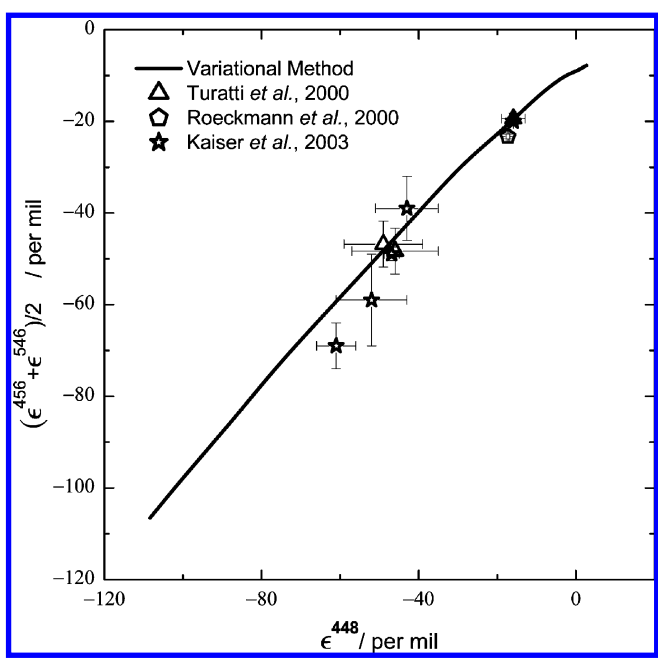


Figure 8. The plot of multi-isotope correlations between the fractionation 448 and the average of the fractionations 456 and 546.

Conclusions

Building on our previous treatment, ^{7,8} the current calculations now include fully 3-dimensional ab initio surfaces, as well as a treatment of the anharmonicity of the experimental ground electronic potential ¹³ in the vibrational wave functions calculated by the variational method. In comparison with the von Hessberg et al. experiment, ⁵ these improvements in the current theory give better agreement in the absorption cross section in the lower energy region. It gave notable improvement in fractionation for the 546 isotopomer and marginal changes for 556 and 456. The improvement is attributed mainly to the more accurate ab initio surfaces that have the dependence on the NN-stretching and some improvement due to anharmonic corrections using the experimental ground electronic potential.

Quantum yield measurements for wavelengths longer than 200 nm (50 000 cm⁻¹), as well as measurements of the

absorption spectrum for 447 and 448 relative to 446 would be useful to understand the difference between the absorption spectra and product yield experimental results. A measurement of the anomalous isotopic fractionation quantity, $^{17}\Delta_{\epsilon}$, with low energy (<51 000 cm $^{-1}$) and narrow bandwidth light sources would be helpful in the comparison of calculations and experiment, in seeing whether the N₂O photolysis has the presently calculated slope (0.537), as compared with the conventional "mass-dependent" value (0.515).

Appendix

The $\mathscr G$ and $\mathscr F$ Matrices. The $\mathscr G$ and $\mathscr F$ matrices of N^1N^2O are defined as in Wilson et al. ¹⁴ We give it here to identify the various constants.

$$\frac{\mathcal{G}}{\left|\frac{1}{m_{N^{1}}} + \frac{1}{m_{N^{2}}} - \frac{-1}{m_{N^{2}}} - 0\right|} = 0$$

$$\frac{-1}{m_{N^{2}}} - \frac{1}{m_{N^{2}}} + \frac{1}{m_{O}} - 0$$

$$0 - 0 - \frac{1}{m_{N^{1}}(r_{NN}^{eq})^{2}} + \frac{1}{m_{N^{2}}} \left(\frac{1}{r_{NN}^{eq}} + \frac{1}{r_{NO}^{eq}}\right)^{2} + \frac{1}{m_{O}(r_{NO}^{eq})^{2}}\right)$$
(12)

$$\mathcal{F} = \begin{pmatrix} k_{\text{NN,NN}} & k_{\text{NN,NO}} & 0 \\ k_{\text{NN,NO}} & k_{\text{NO,NO}} & 0 \\ 0 & 0 & k_{\theta,\theta} \end{pmatrix}$$
 (13)

The mass of each isotope is available from Lide.³¹ The equilibrium NN and NO distances for N₂O are 1.1273 and 1.1851 Å, respectively, which have been obtained in the literature by minimum residual fitting of the rotational and vibrational spectrum of various isotopomers Teffo and Chédin.¹³ The force constants for N₂O in eq 13 are $k_{\rm NN,NN}=18.251$ aJ/Å²; $k_{\rm NO,NO}=11.959$ aJ/Å²; $k_{\rm NN,NO}=1.028$ aJ/Å²; and $k_{\theta,\theta}=0.6659$ aJ/rad².¹³ The \mathcal{L} -matrix is obtained by solving the eigenvectors of the \mathcal{L} -matrix.¹⁴

Harmonic Vibration Wave Functions. For symmetric and asymmetric stretching, the normalized vibrational wave functions are given by

$$\phi_{\nu_i} = \frac{1}{(2^{\nu_i} \nu_i!)^{1/2}} \left(\frac{\alpha_i}{\pi}\right)^{1/4} H_{\nu_i}(\alpha_i^{1/2} q_i) \exp(-\alpha_i q_i^2 / 2)$$
(14)

where $\alpha_i = \omega_i/\hbar$; i equals 1 and 2 for symmetric and asymmetric stretching, respectively; ν_i is the vibrational quantum number; ω_i and q_i are the vibrational angular frequency and the normal mode coordinate, respectively; and $H_{\nu_i}(\alpha_i^{1/2}q_i)$ is a Hermite polynomial. The corresponding vibrational energy for ϕ_{ν_i} is $E_{\nu_i} = 2\pi(\nu_i + 1/2)h\omega_i$.

Since the equilibrium structure of N_2O in the ground electronic state is linear, the normalized wave functions of the degenerate harmonic oscillator are given by

$$\phi_{\nu_{3},l}(q_{3},\xi) = \left[\frac{\alpha_{3}\left(\frac{\nu_{3}-|l|}{2}\right)!}{\pi\left(\frac{\nu_{3}+|l|}{2}\right)!}\right]^{1/2} (\alpha_{3}q_{3}^{2})^{|l|/2}e^{il\xi}L_{(\nu_{3}-|l|)/2}^{l}(\alpha_{3}q_{3}^{2}) \times \exp(-\alpha_{3}q_{3}^{2}/2) \quad (15)$$

where $\alpha_3 = \omega_3/\hbar$; l goes from ν_3 , $\nu_3 - 2$, $\nu_3 - 4$ to $-\nu_3$; ξ is a phase coordinate, ω_3 and q_3 are the vibrational angular frequency and the normal mode coordinate for the bending vibration, respectively; ν_3 and l are the vibrational and internal angular momentum quantum numbers, respectively; and $L_n^l(\alpha_3q_3^2)$ is a Laguerre polynomial. The corresponding vibrational energy is $E_{\nu_3} = 2\pi(\nu_3 + 1)h\omega_3$.

The harmonic wave function $\Phi_n^{(0)}$ and energy $E_n^{(0)}$ can be expressed as

$$\Phi_n^{(0)} = \Phi_{(\nu_1, \nu_2, \nu_3, l)}^{(0)} = \phi_{\nu_1} \phi_{\nu_2} \phi_{\nu_3, l}$$
 (16)

$$E_n^{(0)} = E_{(\nu_1,\nu_2,\nu_3,l)}^{(0)} = 2\pi h [(\nu_1 + 1/2)\omega_1 + (\nu_2 + 1/2)\omega_2 + (\nu_3 + 1)\omega_3]$$
 (17)

Acknowledgment. It is a pleasure to acknowledge the support of this research by the National Science Foundation.

Supporting Information Available: The potential energy and transition moment surfaces used in the present calculation. This material is available free of charge via the Internet at http://pubs.acs.org.

References and Notes

- (1) Ravishankara, A. R.; Daniel, J. S.; Portmann, R. W. Science 2009, 326, 123–125.
- (2) Stein, L. Y.; Yung, Y. L. Annu. Rev. Earth Planet. Sci. 2003, 31, 329–356.
 - (3) Cliff, S. S.; Thiemens, M. H. Science 1997, 278, 1774-1776.
 - (4) Heller, E. J. J. Chem. Phys. 1978, 68, 2066-2075.
- (5) von Hessberg, P.; Kaiser, J.; Enghoff, M. B.; McLinden, C. A.; Sorensen, S. L.; Röckmann, T.; Johnson, M. S. *Atmos. Chem. Phys.* **2004**, *4*, 1237–1253.
- (6) McLinden, C. A.; Prather, M. J.; Johnson, M. S. J. Geophys. Res., [Atmos.] 2003, 108, D04305.
- (7) Prakash, M. K.; Weibel, J. D.; Marcus, R. A. J. Geophys. Res., [Atmos.] 2005, 110, D21315, (Part 1).
- (8) Chen, W. C.; Prakash, M. K.; Marcus, R. A. J. Geophys. Res., [Atmos.] 2008, 113, D05309, (Part 2).
- (9) Schinke, R. *Photodissociation Dynamics*; Cambridge University Press: New York, 1993.
- (10) Johnson, M. S.; Billing, G. D.; Gruodis, A.; Janssen, M. H. M. J. *Phys. Chem. A* **2001**, *105*, 8672–8680.
- (11) Nanbu, S.; Johnson, M. S. J. Phys. Chem. A 2004, 108, 8905–8913.
 - (12) Yung, Y. L.; Miller, C. E. Science 1997, 278, 1778–1780.
- (13) Teffo, J. L.; Chédin, A. J. Mol. Spectrosc. **1989**, 135, 389–409.
- (14) Wilson, E. B.; Decius, J. C.; Cross, P. C. *Molecular Vibrations: The Theory of Infrared and Raman Vibrational Spectra*; McGraw-Hill: New York, 1955.
- (15) Because an isotope substitution would slightly change the absorption cross section in all vibrational states and the changes may not solely depend on the zero point energy (ZPE), calling it a vibrational effect is better than a ZPE effect.
- (16) Choosing the mass-weighted cosine of the bending angle as the q_N is prompted in part because the linear N₂O molecule with fixed NN and NO bond length is a local minimum in the ground electronic surface, but a local maximum in the excited surface.^{26,11}
 - (17) Sovkov, V. B.; Ivanov, V. S. Opt. Spectrosc. 1998, 85, 839-846.
- (18) The ab initio results of Nanbu and Johnson predict the equilibrium NN and NO distance of N_2O in the electronic ground state to be 1.1345 and 1.1885 Å, respectively. Both lengths are slightly longer than experi-

mental results of Teffo and Chédin,¹³ listed in the Appendix. However, any slight shifts of the surfaces to obtain full agreement with the equilibrium structure made a negligible change in the absorption cross section and in the most fractionations, except a few fractionations (7 per mil) in the very low energy region. Therefore, the present calculational results are obtained without any horizontal shifts of the surfaces.

- (19) Zhang, H.; Wennberg, P. O.; Wu, V. H.; Blake, G. A. *Geophys. Res. Lett.* **2000**, 27, 2481–2484.
- (20) Turatti, F.; Griffith, D. W. T.; Wilson, S. R.; Esler, M. B.; Rahn, T.; Zhang, H.; Blake, G. A. *Geophys. Res. Lett.* **2000**, *27*, 2489–2492.
- (21) Röckmann, T.; Brenninkmeijer, C. A. M.; Wollenhaupt, M.; Crowley, J. N.; Crutzen, P. J. *Geophys. Res. Lett.* **2000**, *27*, 1399–1402.
- (22) Röckmann, T.; Kaiser, J.; Crowley, J. N.; Brenninkmeijer, C. A. M.; Crutzen, P. J. *Geophys. Res. Lett.* **2001**, *28*, 503–506.
- (23) Kaiser, J.; Röckmann, T.; Brenninkmeijer, C. A. M.; Crutzen, P. J. *Atmos. Chem. Phys.* **2003**, *3*, 303–313.
- (24) Yoshino, K.; Freeman, D. E.; Parkinson, W. H. *Planet. Space Sci.* **1984**, *32*, 1219–1222.
 - (25) Borges, I. Chem. Phys. 2006, 328, 284-290.

- (26) Daud, M. N.; Balint-Kurti, G. G.; Brown, A. J. Chem. Phys. 2005, 122, 054305.
- (27) Hanisco, T. F.; Kummel, A. C. J. Phys. Chem. 1993, 97, 7242–7246.
- (28) Okabe, H. *Photochemistry of Small Molecules*; John Wiley: New York, 1978.
 - (29) Rahn, T.; Wahlen, M. Science 1997, 278, 1776-1778.
- (30) Minschwaner, K.; Salawitch, R. J.; McElroy, M. B. J. Geophys. Res., [Atmos.] 1993, 98, 10543–10561.
- (31) CRC Handbook of Chemistry and Physics; 84th ed.; Lide, D. R., Ed.; CRC Press: Boca Raton, FL, 2004.
 - (32) Toth, R. A. J. Opt. Soc. Am. B 1986, 3, 1263-1281.
 - (33) Amiot, C. J. Mol. Spectrosc. 1976, 59, 380-395.
- (34) Jolma, K.; Kauppinen, J.; Horneman, V. M. J. Mol. Spectrosc. 1983, 101, 278–284.
 - (35) Toth, R. A. J. Opt. Soc. Am. B 1987, 4, 357-374.

JP101691R